

Statistical Origin of Constituent-Quark Scaling in the QGP hadronization

Zebo Tang^a, Li Yi^{a,b}, Lijuan Ruan^c, Ming Shao^a, Hongfang Chen^a, Cheng Li^a, Bedangadas Mohanty^d, Paul Sorensen^c, Aihong Tang^c, Zhangbu Xu^c

^aUniversity of Science & Technology of China, Hefei 230026, China

^bPurdue University, West Lafayette, Indiana 47907, USA

^cBrookhaven National Laboratory, Upton, New York 11973, USA

^dVariable Energy Cyclotron Centre, 1/AF, Bidhan Nagar, Kolkata 700064, India

Abstract

Nonextensive statistics in a Blast-Wave model (TBW) is implemented to describe the identified hadron production in relativistic p+p and nucleus-nucleus collisions. Incorporating the core and corona components within the TBW formalism allows us to describe simultaneously some of the major observations in hadronic observables at the Relativistic Heavy-Ion Collider (RHIC): the Number of Constituent Quark Scaling (NCQ), the large radial and elliptic flow, the effect of gluon saturation and the suppression of hadron production at high transverse momentum (p_T) due to jet quenching. In this formalism, the NCQ scaling at RHIC appears as a consequence of non-equilibrium process. Our study also provides concise reference distributions with a least χ^2 fit of the available experimental data for future experiments and models.

Keywords:

Tsallis Statistics, non-equilibrium, nonextensive, Quark-Gluon Plasma, Constituent Quark Scaling, perfect liquid, anisotropic flow, jet quenching, Blast-Wave model

Several intriguing features were discovered in relativistic heavy ion collisions [1, 2, 3, 4] when particles emerging from the Quark-Gluon Plasma were detected by the experiments at RHIC. In Au+Au collisions, identified particle yields integrated over the transverse momentum range around the center-of-mass rapidity window have been shown to be at equilibrium at the chemical freeze-out in a statistical analysis [1, 5]. The hydrodynamic model with proper equation of state and initial condition can describe the anisotropic flow with small shear viscosity and provides the notion of "perfect liquid" [6, 7]. Furthermore, the transverse momentum distributions of identified particles can be described in a hydrodynamic-inspired model with a compact set of parameters [1, 5, 8, 9, 10].

However, in the intermediate p_T range, particle production exhibits grouping between baryons and mesons with baryons having relatively higher yield and larger elliptic flow than the mesons [1, 11]. This feature of constituent quark scaling is not present in the hydrodynamics. A microscopic quark coalescence at the hadronization seems to be inescapable [4, 12]. At even higher p_T , hard perturbative QCD processes (jets) are relevant. Absorption of jets in the medium formed in A+A collisions has been used for studying the properties of the QGP [3, 13, 14]. Even though hydrodynamics with space-time evolution from an initial condition [6] is so far the most realistic simulation for bulk matter produced in relativistic heavy ion collisions, its applicability is expected to breakdown for p+p and peripheral A+A collisions at RHIC. Recent study

showed that hydrodynamics can not replace the microscopic hadronic cascade at the late stage regardless of freeze-out and equation of state one chooses [15] because the particle interactions may be dominated by non-equilibrium hadronic processes [16]. In A+A collisions, the fluctuations at initial impact due to Color-Glass Condensate (CGC) formation or individual nucleon-nucleon collision may not be completely washed out by subsequent interactions in either the QGP phase or hadronic phase [17]. These effects leave footprints in the spectra at low and intermediate p_T .

With its development and success of nonextensive statistics (also known as Tsallis statistics [18]) in dealing with non-equilibrated complex systems in condensed matter, many authors have utilized Tsallis statistics to understand the particle production in high-energy and nuclear physics [10, 19, 20, 21, 22, 23]. Although the implications and understanding of the consequences of such an application are still under investigation, the usual Boltzmann distribution in an m_T exponential form can be readily re-written as an m_T power-law (Levy) function [24]:

$$\frac{d^2N}{2\pi m_T dm_T dy} \propto \left(1 + \frac{q-1}{T} m_T\right)^{-1/(q-1)} \quad (1)$$

where the left-hand side is the invariant differential particle yield and q is a parameter characterizing the degree of non-equilibrium, $m_T = \sqrt{m^2 + p_T^2}$ is the transverse mass of the given particle with mass of m and T is related to the temperature of the system. The distribution can be derived from the usual procedure in statistical mechanics, starting from a non-

Email address: zbtang@ustc.edu.cn (Zebo Tang)

equilibrium q -entropy [18]. The successful application of Levy functions (TBW_{pp}) to the spectra in p+p collisions at RHIC resulted in q values significantly larger than unity and are different between the groups of baryons and mesons [10, 25]. However, in the central Au+Au collisions, the spectra at low p_T show characteristic Boltzmann distribution with q value being close to unity ($q \rightarrow 1$, Eq. 1 becomes a Boltzmann distribution) even though there are still significant power-law tails with considerable particle yields at high p_T [10]. In addition to the escaping jets at high p_T , coalescence with non-equilibrated quarks has also been proposed to study the power-law behavior [26]. Difficulty in accounting for these processes so far seems to be a major limitation of the TBW statistical description of the experimental data over a wide p_T range [10]. To bridge the hydrodynamic nature of the spectra at low p_T and power-law tails at high p_T with smooth transition at intermediate p_T , models which include a hot and dense core with a corona of jet-like process have been proposed [14, 27].

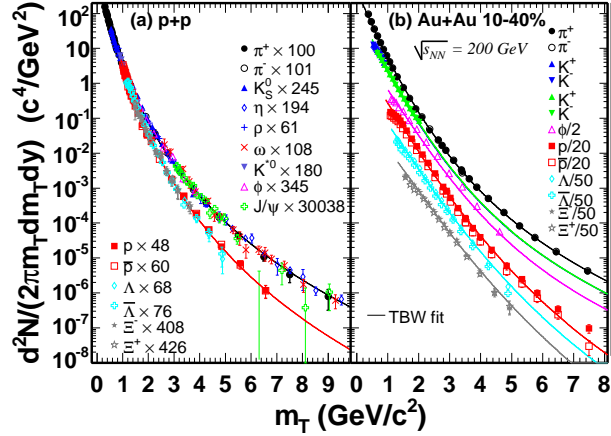


Figure 1: (Color Online) Identified particle transverse mass spectra in p+p collisions (a) and 10-40% Au+Au collisions (b) at $\sqrt{s_{NN}} = 200$ GeV. The symbols represent experimental data points. The curves represent the TBW fit. Only fits to the particles are shown since the model has the same spectral shapes for particles and anti-particles. For plotting in panel (a), the spectra of meson (baryon) are scaled to match that of π^+ (p) at $m_T = 1.5$ GeV/ c^2 for ϕ (Ξ^\pm), at 4 GeV/ c^2 for J/ψ and at 1 GeV/ c^2 for the rest.

In this paper, we present the procedure of implementing nonextensive statistics in the Blast-Wave model (TBW) with azimuthally anisotropic particle emission, and use it to fit the identified particle spectra and for the first time to elliptic flow at mid-rapidity at RHIC. The model uses the TBW function obtained from p+p data [10] as corona and an additional TBW function as core to fit Au+Au data. The formalism thus provides a systematic comparison between p+p and central A+A collisions in one macroscopic statistical model framework and gives an accurate numeric description of the experimental data over a wide range of p_T . Examples of such successful applications in the related subjects are the chemical fit to the particle yields [28, 29] and the global fit of the parton distribution function (PDF) of proton [30]. Good TBW fits can also offer a simple formula for developing ideas and building models in a reasonably realistic environment [5, 8, 9, 14, 31, 32, 33, 34], and provide a practical experimental tool to extract particle yields

by extrapolating to unmeasured kinematic ranges.

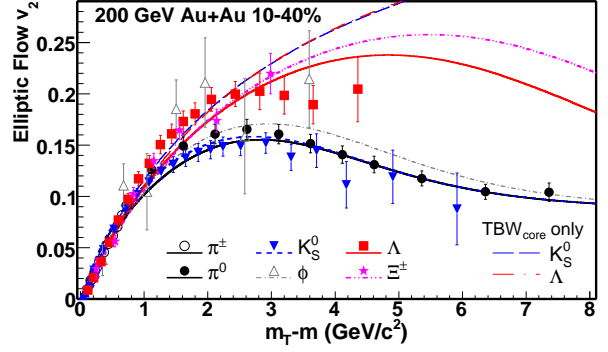


Figure 2: (Color Online) Identified particle v_2 in 10-40% Au+Au collisions. The x-axis is depicted by the kinetic energy ($m_T - m$) [7], showing the scaling of v_2 at low p_T , and grouping of baryons and mesons at the intermediate p_T range. The curves represent the TBW fit (Eq. 3) and the characteristic NCQ scaling. Also shown are the indistinguishable K_S^0 and Λ curves from TBW_{core} alone over the entire range.

To take into account collective flow and azimuthal anisotropy in the transverse direction in relativistic heavy ion collisions, Levy distribution needs to be embedded in the framework of hydrodynamic expansion [20]. We follow the recipe of the Blast-Wave model provided in literature [5, 8, 9, 34], and change sources of particle emission from a Boltzmann distribution to a Levy distribution [10]:

$$\frac{dN}{m_T dm_T d\phi} \propto m_T \int_0^{2\pi} d\phi_s \int_{-y_b}^{+y_b} dy e^{\sqrt{y_b^2 - y^2} \cosh(y)} \times \int_0^R r dr (1 + \frac{q-1}{T} E_T)^{-1/(q-1)}, \quad (2)$$

where $y_b = \ln(\sqrt{s_{NN}}/m_N)$ [35] is the beam rapidity and the rapidity distribution can be approximated as a Gaussian with a width of $\sigma_y = 2.27 \pm 0.02$ at the center-of-mass energy of $\sqrt{s_{NN}} = 200$ GeV [36, 37], transverse energy $E_T = m_T \cosh(y) \cosh(\rho) - p_T \sinh(\rho) \cos(\phi_b - \phi)$, $\rho = \sqrt{(r \cos(\phi_s)/R_X)^2 + (r \sin(\phi_s)/R_Y)^2} (\rho_0 + \rho_2 \cos(2\phi_b))$ is the flow profile in transverse rapidity, and $\tan(\phi_b) = (R_X/R_Y)^2 \tan(\phi_s)$ relates the azimuthal angle of the coordinate space (ϕ_s) to the angle of the flow direction (ϕ_b) of the emitting source [9]. Equation 2 extends the nonextensive statistics in a blast-wave model [10] to incorporate particle emission from an elliptic source (R_X and R_Y are the axes in the coordinate space) with an elliptic expansion (ρ_0 and ρ_2) [9]. In addition to this core component, it is important to include the corona with jet-like particle emission at high momentum resembling an ensemble of individual p+p collisions [14, 27]. The combined core and corona formula reads:

$$\frac{dN}{m_T dm_T d\phi} \Big|_{AA} = TBW_{core} + f_{pp} N_{bin} \epsilon (1 + v_2^{jet} \cos(2\phi)) TBW_{pp}, \quad (3)$$

where TBW_{core} is from Eq. 2, f_{pp} and v_2^{jet} represent the fraction and the anisotropy of the escaping jet comparing to the expected number of binary p+p collisions in Au+Au collisions

Table 1: Values of parameters and best χ^2 from TBW fit of Eq. 4 to identified particle p_T spectra in $p+p$ collisions at RHIC. The uncorrelated systematic errors are included in the fit.

	T (MeV)	$q - 1$	χ^2/nDoF
Mesons	89.9 ± 0.7	0.0955 ± 0.0006	283/257
Baryons	68.5 ± 4.0	0.0855 ± 0.0019	151/128

(N_{bin}), $\epsilon = p_T^2/(p_T^2 + Q_S^2)$ takes into account the gluon saturation effect from $p+p$ to Au+Au collisions with saturation scale $Q_S = 1.5 \text{ GeV}/c$ [38], and TBW_{pp} are the adopted fit results from the spectra in $p+p$ collisions without any additional free parameter for either baryons or mesons. Since radial flow velocity ρ was found to be zero in $p+p$ collisions [10], TBW_{pp} can be simplified as:

$$TBW_{pp} \propto m_T \int_{-y_b}^{+y_b} dy e^{\sqrt{y_b^2 - y^2}} \cosh(y) \times (1 + \frac{q-1}{T} m_T \cosh(y))^{-1/(q-1)}, \quad (4)$$

The STAR and PHENIX collaborations have published the most complete series of particle spectra and v_2 at mid-rapidity for $p+p$ and Au+Au collisions at $\sqrt{s_{NN}} = 200 \text{ GeV}$. The identified particle spectra and v_2 include π^\pm , K^\pm , K_S , K^* , p , ϕ , Λ , Ξ^- , \bar{p} , $\bar{\Lambda}$, and Ξ^+ in STAR publications [1, 5, 39, 40, 41, 42, 43, 44, 45, 46, 47, 48, 49, 50]. The η , η' and ω spectra in $p+p$ collisions, K^\pm spectra and π^0 v_2 in Au+Au collisions are from PHENIX publications [51, 52, 53, 54, 55, 56]. Figure 1.a shows the invariant differential yields in $p+p$ collisions at $\sqrt{s} = 200 \text{ GeV}$. All of the mesons or baryons have the common m_T spectra shape. The solid lines represent the fit to Eq. 4 for mesons and baryons separately. The common fit parameters and best χ^2 per fitting degree of freedom (nDoF) are listed in Tab. 1. In addition to the common fit parameters, a global normalization factor was applied for each particle spectrum. The p_T -integrated cross section $d\sigma/dy$ for each particle species obtained from the fit are listed in Tab. 2. Figure 1.b shows the invariant differential yields together with our fit results in 10-40% centrality Au+Au collisions. The results of v_2 from the simultaneous fit with spectra are displayed in Fig. 2. The fit parameters and best χ^2 per nDoF are tabulated in Tab. 3. In addition to these parameters common to all particles, a fit parameter is required as a normalization factor for TBW_{core} of each particle spectrum. The TBW_{pp} in the fit function is directly adopted from the fit results shown in Fig. 1.a for each particle species without any additional free parameter. The R_{AA} (ratio of the N_{bin} normalized p_T spectra in A+A collisions to the underlying $p+p$ spectrum) from model reproduces the data very well, as shown in Fig. 3.

The Blast-Wave model with nonextensive statistics and azimuthal anisotropy and a core-corona composition has allowed high quality fits to spectra and elliptic flow over a broad p_T range. The striking feature of the experimental observations related to the NCQ scaling is well reproduced. The results can be summarized as follows: 1) The bulk core alone (TBW_{core}) with finite q value can fit the data very well at low p_T [10, 16]. The new extension to v_2 continues to provide high quality fits. The system produces maximum radial flow velocities of

$\tanh(\rho_0 + \rho_2) = 0.69c$ and $\tanh(\rho_0 - \rho_2) = 0.43c$ along x-axis (the reaction plane) and y-axis, respectively. This demonstrates that the bulk system can be described with a few macroscopic parameters and is qualified as a thermodynamic state. 2) Figure 3 shows that the R_{AA} of the experimental data points at low p_T are below those at high p_T . The ϵ parameter necessarily brings the $p+p$ component at low p_T down to a subdominant fraction. This necessity may be partly due to the modification of the jet low- p_T component by the bulk [14]. 3) The non-equilibrated component in the bulk core produces a power-law tail in spectra and high v_2 at the intermediate p_T . 4) The baryon and meson yields (TBW_{pp}) are grouped in $p+p$ collisions with baryon yields systematically lower than meson yields as observed in the experimental data [10, 27, 41]. 5) The combination of non-equilibrium tail from core and the baryon-meson separation from corona brings down the bulk v_2 , produces the baryon enhancement and the NCQ scaling at the intermediate p_T . 6) The medium quenches the jet and reduces it to a fraction ($f_{pp} = 0.36$) of its underlying binary nucleon-nucleon collisions, resulting in a finite azimuthally anisotropic emission ($v_2^{jet} = 8.7\%$) [60]. 7) The high-precision ($\pm 10^{-4}$ stat.) experimental data points concentrate at low p_T , dominating the fit χ^2 . Additional high-quality data in higher p_T range (e.g. v_2 of baryons) will balance the contributions to the χ^2 from components with different physical origins. The not-ideal χ^2/nDoF value indicates significant tensions among the different datasets and model, and warrants further detailed assessment and categorization similar to the PDF fit [61] in the future.

This TBW model describes the number of constituent quark (NCQ) dependencies observed in the data which have also been described in recombination models [4, 12, 26, 62]. The NCQ dependence indicates that baryon production at intermediate p_T increases faster going from $p+p$ to Au+Au collisions than meson production does. The division into a core and corona component in Eq. 3 represents a division into two samples: a core and corona where the core has a larger fraction of baryons than the corona. We describe both the core and corona with a TBW statistical model. But whereas the recombination picture attempts to provide a microscopic description for why the bulk in

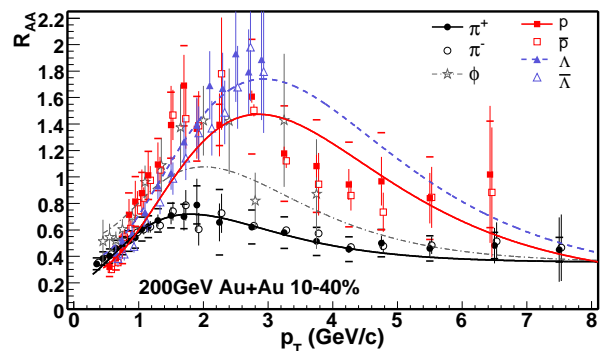


Figure 3: (Color Online) Comparison of TBW fit (lines) with STAR measurements of R_{AA} in 10-40% Au+Au collisions. The syst. errors (horizontal bars) and stat. errors (vertical lines) are shown separately for protons and charged pions. Systematic and statistical errors are added quadratically in the fit, and are shown as such in the plot except the protons and charged pions.

Table 2: Cross sections $d\sigma/dy$ in mb of different particles at mid-rapidity in $p+p$ collisions at $\sqrt{s_{NN}} = 200$ GeV. “ TBW_{pp} ” column show the values obtained from fit results shown in Fig. 1.a. “Data Ref.” column shows where are the data points from. “PHENIX” column shows the values obtained by fits to PHENIX measured spectra with the Tsallis functional form as described in Ref. [56]. “Published” column shows the values published by experiments. An additional 9.7% systematic uncertainty should be added to all $d\sigma/dy$ values listed in the column “PHENIX” and 12% to the values in the column “STAR” to account for the trigger uncertainties. Values in the column “Published” are also given without these systematic uncertainties. The column “S.M.” is the prediction of the statistical model [57]. All errors are the combined statistical and systematic uncertainties.

Particle	TBW_{pp}	Data Ref.	PHENIX [56]	STAR	S.M. [57]
π^0			41.4 ± 5.8		46.9
π^+	42.4	[5, 47]	39.4 ± 7.3	43.2 ± 3.3 [34]	42.1
π^-	41.9	[5, 47]	38.6 ± 7.2	42.6 ± 3.3 [34]	41.5
K^+	4.69	[5, 44, 41]	4.57 ± 0.61	4.50 ± 0.39 [34]	4.57
K^-	4.57	[5, 44, 41]	4.20 ± 0.51	4.35 ± 0.39 [34]	4.38
K_S^0	4.73	[41]	5.28 ± 0.53	4.02 ± 0.34 [41]	4.40
η	4.94	[51]	4.47 ± 0.96		4.93
ρ	6.79	[50]		7.8 ± 1.2 [50]	5.58
ω	3.75	[52]	3.65 ± 0.77		5.03
η'	0.58	[56]	0.62 ± 0.17		0.365
$(K^{*+} + K^{*-})/2$	1.51	[39]			1.57
$(K^{*0} + \bar{K}^{*0})/2$	1.54	[39]		1.52 ± 0.19 [39]	1.55
ϕ	0.521	[45]	0.421 ± 0.055	0.540 ± 0.086 [45]	0.339
$J/\psi (\times 10^3)$	0.741	[53]	0.759 ± 0.053		
$\psi' (\times 10^3)$			0.133 ± 0.031		
p	3.96	[5, 47]		4.14 ± 0.30 [34]	4.47
\bar{p}	3.19	[5, 47]		3.39 ± 0.36 [34]	3.59
Λ	1.36	[41]		1.31 ± 0.12 [41]	1.30
$\bar{\Lambda}$	1.21	[41]		1.19 ± 0.11 [41]	1.11
Ξ^-	0.098	[41]		0.078 ± 0.028 [41]	0.092
$\bar{\Xi}^+$	0.094	[41]		0.087 ± 0.031 [41]	0.082
$\Sigma^{*+} + \Sigma^{*-}$	0.359	[58]		0.321 ± 0.044 [58]	0.308
$\bar{\Sigma}^{*+} + \bar{\Sigma}^{*-}$	0.313	[58]		0.267 ± 0.038 [58]	0.260
$\bar{\Lambda}^* + \Lambda^*$	0.125	[58]		0.104 ± 0.017 [58]	0.168
$\Omega^- + \bar{\Omega}^+ (\times 10^3)$	12.3	[41]		10.2 ± 5.7 [41]	17.1

Table 3: Values of parameters and best χ^2 from TBW fit of Eq. 3 to identified particle p_T spectra and v_2 in 10-40% Au+Au collisions at RHIC. The uncorrelated systematic errors are included in the fit. Syst. error of STAR $v_2\{EP\}$ are taken to be $15\% / \sqrt{12}$ [48]. The spectra contribute 359/244 to the χ^2/nDoF . $Q_S = 2.1 \pm 0.2$ GeV/c with $\chi^2/\text{nDoF}=497/295$ when Q_S is a free parameter. Including the $v_2\{EP\}$ of K^\pm and \bar{p} at low p_T [59] increases the best χ^2/nDoF to 769/307.

ρ_0	ρ_2	R_X/R_Y	T (MeV)	$q - 1$	f_{pp}	v_2^{jet}	χ^2/nDoF
0.654 ± 0.002	0.199 ± 0.002	0.871 ± 0.004	128 ± 2	0.044 ± 0.001	0.36 ± 0.01	$(8.7 \pm 0.4) \%$	506/296

Au+Au collisions has a larger fraction of baryons, the macroscopic TBW statistical model only describes the existing states as they are, and is not sensitive to the underlying mechanism responsible for producing those states. Regardless of whether the TBW_{pp} component is indeed from individual p+p collision or part of the hadrons from coalescence of the escaping partons, Eq. 3 does provide a unified tool to describe simultaneously a variety of measurements over a wide range in p_T for future studies. These results also provide a macroscopic foundation for discussing the entropy issues associated with the system’s underlying microscopic subprocesses [23, 26, 63, 64].

In summary, we have implemented the nonextensive statistics in a Blast-Wave model and incorporated a core-corona model to describe a complete data set on identified particle spectra and elliptic flow versus transverse momenta at mid-rapidity measured at RHIC. Such a formalism simultaneously describes several novel observations reported at RHIC over a

broad p_T range. Specifically it provides an alternative physical picture, through the role of the core-corona and non-equilibrium effects in understanding the baryon-meson differences in the nuclear modification factor and the elliptic flow at intermediate p_T . The macroscopic nonextensive statistics provides a complementary microscopic method to the hydrodynamics and hadronic cascade for studying the evolution of the nucleus-nucleus collisions and the properties of QGP.

Acknowledgments

The authors thank Dr. Yuting Bai for clarification of STAR $v_2\{2\}$ and $v_2\{EP\}$ data, and Drs. B. Christie, J. Dunlop, J. Liao, V. Koch, Profs. F.Q. Wang, Q. Wang and G. Wilk for discussions. This work was supported in part by the Offices of NP and HEP within the U.S. DOE Office of Science under the contracts of DE-FG02-88ER40412 and DE-AC02-98CH10886. USTC

group is supported in part by NNSF of China under Grant No. 11005103 and 10835005. BM is supported by DAE-BRNS project Sanction No. 2010/21/15-BRNS/2026.

References

- [1] J. Adams, et al., Experimental and theoretical challenges in the search for the quark gluon plasma: The STAR collaboration's critical assessment of the evidence from RHIC collisions, Nucl. Phys. A757 (2005) 102–183. doi:10.1016/j.nuclphysa.2005.03.085.
- [2] K. Adcox, et al., Formation of dense partonic matter in relativistic nucleus nucleus collisions at RHIC: Experimental evaluation by the PHENIX collaboration, Nucl. Phys. A757 (2005) 184–283. doi:10.1016/j.nuclphysa.2005.03.086.
- [3] M. Gyulassy, L. McLerran, New forms of QCD matter discovered at RHIC, Nucl. Phys. A750 (2005) 30–63. doi:10.1016/j.nuclphysa.2004.10.034.
- [4] B. Muller, Hadronic signals of deconfinement at RHIC, Nucl. Phys. A750 (2005) 84–97.
- [5] J. Adams, et al., Identified particle distributions in p p and Au + Au collisions at $s^{*}(1/2) = 200$ -GeV, Phys. Rev. Lett. 92 (2004) 112301. doi:10.1103/PhysRevLett.92.112301.
- [6] P. F. Kolb, U. W. Heinz, Hydrodynamic description of ultrarelativistic heavy-ion collisions arXiv:nucl-th/0305084.
- [7] R. A. Lacey, A. Taranenko, What do elliptic flow measurements tell us about the matter created in the little bang at RHIC?, PoS CFRNC2006 (2006) 021.
- [8] E. Schnedermann, J. Sollfrank, U. W. Heinz, Thermal phenomenology of hadrons from 200-A/GeV S+S collisions, Phys. Rev. C48 (1993) 2462–2475. doi:10.1103/PhysRevC.48.2462.
- [9] F. Retiere, M. A. Lisa, Observable implications of geometrical and dynamical aspects of freeze-out in heavy ion collisions, Phys. Rev. C70 (2004) 044907. doi:10.1103/PhysRevC.70.044907.
- [10] Z. Tang, et al., Spectra and radial flow at RHIC with Tsallis statistics in a Blast-Wave description, Phys. Rev. C79 (2009) 051901.
- [11] R. J. Fries, V. Greco, P. Sorensen, Coalescence Models For Hadron Formation From Quark Gluon Plasma, Ann. Rev. Nucl. Part. Sci. 58 (2008) 177–205.
- [12] V. Greco, C. M. Ko, P. Levai, Parton coalescence and antiproton/pion anomaly at RHIC, Phys. Rev. Lett. 90 (2003) 202302.
- [13] H. Zhang, J. F. Owens, E. Wang, X.-N. Wang, Dihadron Tomography of High-Energy Nuclear Collisions in NLO pQCD, Phys. Rev. Lett. 98 (2007) 212301. doi:10.1103/PhysRevLett.98.212301.
- [14] J. Liao, V. Koch, Exposing the non-collectivity in elliptic flow, Phys. Rev. Lett. 103 (2009) 042302.
- [15] H. Song, S. A. Bass, U. W. Heinz, Viscous QCD matter in a hybrid hydrodynamic+Boltzmann approach arXiv:arXiv:1012.0555.
- [16] M. Shao, et al., Examine the species and beam-energy dependence of particle spectra using Tsallis Statistics, J. Phys. G37 (2010) 085104.
- [17] H. J. Drescher, S. Ostapchenko, T. Pierog, K. Werner, Initial condition for QGP evolution from NEXUS, Phys. Rev. C65 (2002) 054902. doi:10.1103/PhysRevC.65.054902.
- [18] C. Tsallis, Possible Generalization of Boltzmann-Gibbs Statistics, J. Stat. Phys. 52 (1988) 479–487. doi:10.1007/BF01016429.
- [19] B. De, S. Bhattacharyya, G. Sau, S. K. Biswas, Non-extensive thermodynamics, heavy ion collisions and particle production at RHIC energies, Int. J. Mod. Phys. E16 (2007) 1687–1700. doi:10.1142/S0218301307006976.
- [20] G. Wilk, Z. Włodarczyk, Power laws in elementary and heavy-ion collisions: A Story of fluctuations and nonextensivity?, Eur. Phys. J. A40 (2009) 299–312.
- [21] W. M. Alberico, A. Lavagno, P. Quarati, Non-extensive statistics, fluctuations and correlations in high energy nuclear collisions, Eur. Phys. J. C12 (2000) 499–506.
- [22] T. Osada, G. Wilk, Nonextensive hydrodynamics for relativistic heavy-ion collisions, Phys. Rev. C77 (2008) 044903. doi:10.1103/PhysRevC.77.044903.
- [23] T. S. Biro, B. Muller, Almost exponential transverse spectra from power law spectra, Phys. Lett. B578 (2004) 78–84. doi:10.1016/j.physletb.2003.10.052.
- [24] G. Wilk, Z. Włodarczyk, On the interpretation of nonextensive parameter q in Tsallis statistics and Levy distributions, Phys. Rev. Lett. 84 (2000) 2770. doi:10.1103/PhysRevLett.84.2770.
- [25] A. Adare, et al., Measurement of neutral mesons in p+p collisions at $\sqrt{s}=200$ GeV and scaling properties of hadron production arXiv:arXiv:1005.3674.
- [26] T. S. Biro, G. Purcsel, K. Urmosy, Non-Extensive Approach to Quark Matter, Eur. Phys. J. A40 (2009) 325–340.
- [27] K. Werner, Core-Corona Separation in Ultra-Relativistic Heavy Ion Collisions, Phys. Rev. Lett. 98 (2007) 152301.
- [28] A. Andronic, P. Braun-Munzinger, K. Redlich, J. Stachel, Statistical hadronization of charm in heavy-ion collisions at SPS, RHIC and LHC, Phys. Lett. B571 (2003) 36–44.
- [29] J. Cleymans, G. Hamar, P. Levai, S. Wheaton, Near-thermal equilibrium with Tsallis distributions in heavy ion collisions, J. Phys. G36 (2009) 064018.
- [30] H. L. Lai, et al., Global QCD analysis and the CTEQ parton distributions, Phys. Rev. D51 (1995) 4763–4782.
- [31] X. Zhao, R. Rapp, Transverse Momentum Spectra of J/ψ in Heavy-Ion Collisions, Phys. Lett. B664 (2008) 253–257.
- [32] S. Gavin, L. McLerran, G. Moschelli, Long Range Correlations and the Soft Ridge in Relativistic Nuclear Collisions, Phys. Rev. C79 (2009) 051902.
- [33] E. V. Shuryak, On the Origin of the 'Ridge' phenomenon induced by Jets in Heavy Ion Collisions, Phys. Rev. C76 (2007) 047901. doi:10.1103/PhysRevC.76.047901.
- [34] B. I. Abelev, et al., Systematic Measurements of Identified Particle Spectra in pp , d^+ Au and Au+Au Collisions from STAR, Phys. Rev. C79 (2009) 034909. doi:10.1103/PhysRevC.79.034909.
- [35] C.-Y. Wong, Landau Hydrodynamics Revisited, Phys. Rev. C78 (2008) 054902. arXiv:0808.1294, doi:10.1103/PhysRevC.78.054902.
- [36] I. Bearden, et al., Charged meson rapidity distributions in central Au + Au collisions at $s(NN)^{1/2} = 200$ -GeV, Phys. Rev. Lett. 94 (2005) 162301.
- [37] P. K. Netrakanti, B. Mohanty, Width of the rapidity distribution in heavy-ion collisions, Phys. Rev. C 71 (4) (2005) 047901. doi:10.1103/PhysRevC.71.047901.
- [38] J. Schaffner-Bielich, D. Kharzeev, L. D. McLerran, R. Venugopalan, Generalized scaling of the transverse mass spectrum at the Relativistic Heavy-Ion Collider, Nucl. Phys. A705 (2002) 494–507.
- [39] J. Adams, et al., $K^*(892)$ resonance production in Au + Au and p + p collisions at $s(NN)^{1/2} = 200$ -GeV at STAR, Phys. Rev. C71 (2005) 064902. doi:10.1103/PhysRevC.71.064902.
- [40] B. I. Abelev, et al., Partonic flow and Phi-meson production in Au + Au collisions at $s(NN)^{1/2} = 200$ -GeV, Phys. Rev. Lett. 99 (2007) 112301. doi:10.1103/PhysRevLett.99.072501.
- [41] B. I. Abelev, et al., Strange particle production in p + p collisions at $s^{*}(1/2) = 200$ -GeV, Phys. Rev. C75 (2007) 064901. doi:10.1103/PhysRevC.75.064901.
- [42] B. I. Abelev, et al., Identified baryon and meson distributions at large transverse momenta from Au + Au collisions at $s(NN)^{1/2} = 200$ -GeV, Phys. Rev. Lett. 97 (2006) 152301. doi:10.1103/PhysRevLett.97.152301.
- [43] B. I. Abelev, et al., Energy dependence of π^{\pm} , p and \bar{p} transverse momentum spectra for Au+Au collisions at $\sqrt{s_{NN}} = 62.4$ and 200 GeV, Phys. Lett. B655 (2007) 104–113. doi:10.1016/j.physletb.2007.06.035.
- [44] J. Adams, et al., Pion, kaon, proton and anti-proton transverse momentum distributions from p + p and d + Au collisions at $s(NN)^{1/2} = 200$ -GeV, Phys. Lett. B616 (2005) 8–16. doi:10.1016/j.physletb.2005.04.041.
- [45] J. Adams, et al., Phi meson production in Au + Au and p + p collisions at $s^{*}(1/2) = 200$ -GeV, Phys. Lett. B612 (2005) 181–189. doi:10.1016/j.physletb.2004.12.082.
- [46] J. Adams, et al., Scaling Properties of Hyperon Production in Au+Au Collisions at $\sqrt{s_{NN}} = 200$ GeV, Phys. Rev. Lett. 98 (2007) 062301. doi:10.1103/PhysRevLett.98.062301.
- [47] J. Adams, et al., Identified hadron spectra at large transverse momentum in p + p and d + Au collisions at $s(NN)^{1/2} = 200$ -GeV, Phys. Lett. B637 (2006) 161–169. doi:10.1016/j.physletb.2006.04.032.
- [48] J. Adams, et al., Azimuthal anisotropy in Au + Au collisions at

- $s(NN)^{1/2} = 200$ -GeV, Phys. Rev. C72 (2005) 014904.
- [49] B. I. Abelev, et al., Centrality dependence of charged hadron and strange hadron elliptic flow from $\sqrt{s_{NN}} = 200$ GeV Au+Au collisions, Phys. Rev. C77 (2008) 054901.
- [50] J. Adams, et al., ρ^0 production and possible modification in Au + Au and p + p collisions at $s(NN)^{1/2} = 200$ -GeV, Phys. Rev. Lett. 92 (2004) 092301.
- [51] S. S. Adler, et al., High transverse momentum η meson production in $p^+ p$, d^+ Au and Au+Au collisions at $S(MN)^{1/2} = 200$ -GeV, Phys. Rev. C75 (2007) 024909.
- [52] S. S. Adler, et al., Production of omega mesons at large transverse momenta in p + p and d + Au collisions at $s(NN)^{1/2} = 200$ -GeV, Phys. Rev. C75 (2007) 051902.
- [53] A. Adare, et al., J/ψ production versus transverse momentum and rapidity in $p+p$ collisions at $\sqrt{s} = 200$ GeV, Phys. Rev. Lett. 98 (2007) 232002.
- [54] S. S. Adler, et al., Identified charged particle spectra and yields in Au+Au collisions at $\sqrt{s_{NN}} = 200$ GeV, Phys. Rev. C69 (2004) 034909.
- [55] A. Adare, et al., Azimuthal anisotropy of neutral pion production in Au+Au collisions at $\sqrt{s_{NN}} = 200$ GeV: Path-length dependence of jet quenching and the role of initial geometry, Phys. Rev. Lett. 105 (2010) 142301.
- [56] A. Adare, et al., Measurement of neutral mesons in p+p collisions at $\sqrt{s} = 200$ GeV and scaling properties of hadron production, Phys. Rev. D83 (2011) 052004. arXiv:1005.3674, doi:10.1103/PhysRevD.83.052004.
- [57] F. Becattini, R. Fries, The QCD confinement transition: hadron formation arXiv:0907.1031.
- [58] J. Adams, et al., Strange baryon resonance production in $s(NN)^{1/2} = 200$ -GeV p + p and Au + Au collisions, Phys. Rev. Lett. 97 (2006) 132301. doi:10.1103/PhysRevLett.97.132301.
- [59] Y. Bai, Anisotropic Flow Measurements in STAR at the Relativistic Heavy Ion Collider, NIKHEF and Utrecht University Ph.D.
- [60] J. Liao, E. Shuryak, Angular Dependence of Jet Quenching Indicates Its Strong Enhancement Near the QCD Phase Transition, Phys. Rev. Lett. 102 (2009) 202302.
- [61] H.-L. Lai, M. Guzzi, J. Huston, Z. Li, P. M. Nadolsky, J. Pumplin, C.-P. Yuan, New parton distributions for collider physics, Phys. Rev. D 82 (7) (2010) 074024. doi:10.1103/PhysRevD.82.074024.
- [62] R. C. Hwa, C. B. Yang, Recombination of shower partons at high p(T) in heavy-ion collisions, Phys. Rev. C70 (2004) 024905.
- [63] M. He, R. J. Fries, R. Rapp, Scaling of Elliptic Flow, Recombination and Sequential Freeze-Out of Hadrons in Heavy-Ion Collisions, Phys. Rev. C82 (2010) 034907.
- [64] O. J. E. Maroney, Thermodynamic constraints on fluctuation phenomena, Phys. Rev. E 80 (6) (2009) 061141. doi:10.1103/PhysRevE.80.061141.